KSCE Journal of Civil Engineering (2021) 25(10):3879-3896
DOI 10.1007/s12205-021-2161-8

pISSN 1226-7988, eISSN 1976-3808
www.springer.com/12205

Structural Engineering

Seismic Performance Analysis of Buckling-Restrained Braced Steel Frames with Ductile Castings

Zhanzhong Yin[a,b], **Bo Yang**[a], **and Shuzhen An**[a]

[a]*School of Civil Engineering, Lanzhou University of Technology, Lanzhou730050, China*
[b]*Western Engineering Research Center of Disaster Mitigation in Civil Engineering of Ministry of Education, Lanzhou University of Technology, Lanzhou 730050, China*

ARTICLE HISTORY

Received 7 December 2020
Revised 17 March 2021
Accepted 25 April 2021
Published Online 23 June 2021

KEYWORDS

Concentrically braced steel frames
Ductile castings
Quasi-static test
Buckling-restrained brace
Energy dissipation performance

ABSTRACT

Buckling-restrained brace (BRB) steel frames with ductile castings are proposed to solve the fracture failure of welded joints between buckling-restrained braces and frames after rare earthquakes. In this paper, quasi-static tests are conducted on two one-story, one-bay steel frames to study their mechanical behaviors, including stress distribution, failure mode, energy dissipation, and skeleton curve, and finite element models are established for verification. Subsequently, 22 models with different parameters of the BRB steel frames with ductile castings are analyzed using ABAQUS. Results indicate that the new frame system has good energy dissipation; it can confine the inelastic deformation of the structure to the ductile castings and BRB. It also satisfies the 1/50 maximum elastic-plastic drift angle set by the Code for Seismic Design of Buildings. The BRB with ductile castings connected to the frames by bolts can relieve the stress distribution in the beam–column region, which can be assembled and replaced after the earthquake.

1. Introduction

Special concentrically braced frames (SCBFs) are structural system with good seismic performance which have a large lateral stiffness, higher bearing capacity and better ductility (Uriz, 2005). The brace and the frame are generally designed to be welded in the design of the structure, which makes the stress concentration in the joint field of SCBFs. And it is easy to generate the three-axis stress field and cause the brittle fracture in the gusset plate, which will compromise the energy dissipation capacity of the brace (Powell, 2009). The occurrence of major earthquakes has also exposed the problem that the performance of the SCBFs cannot be given full play due to design and construction defects (Tremblay et al., 1995; Hsiao, 2012). To address above problems, scholars have done a lot of research (Popov et al., 1976; Black et al., 1980; Foutch et al., 1987). Astaneh-Asl et al. (1989), El-Tayem and Goel (1985), Xu (1990) studied the whole SCBF system, which was composed of the brace with gusset plate connection, and found that the gusset plate and beam-column joints were prone to brittle failure. Uriz and Mahin (2004) investigated the seismic performance of concentrically braced frames. They concluded that SCBFs are subject to severe strength deterioration and brace fracture in an experimental study on a full-size, two-story SCBF including HSS cross section brace and tapered gusset plate. Lehman and Roeder (2008) studied the performance of special concentrically braced frames, the research showed that the deformation capacity of brace was limited by its yield. Roeder et al. (2011a, 2011b) studied seismic design of SCBFs, and concluded that balancing the yield and buckling of braces and the yield of joints can improve the lateral displacement of the structure, and puts forward to Balanced Design Procedure method of SCBFs, improving the ductility of the structure, to delay the occurrence of potential failure mode. According to the “dog bone” design concept (Balut and Gioncu, 2003), Ward et al. (2012) introduced a cast modular ductile bracing system as an alternative to special concentrically braced frames. Through an analytical research of capacity parameters, relevant design suggestions were given. To improve the ductility of BRBs and reduce the damage of the joint between the brace and the frame, Gray et al. (2010, 2014) designed a cast steel

CORRESPONDENCE Zhanzhong Yin yzztianyu@126.com School of Civil Engineering, Lanzhou University of Technology, Lanzhou 730050, China; Western Engineering Research Center of Disaster Mitigation in Civil Engineering of Ministry of Education, Lanzhou University of Technology, Lanzhou 730050, China

yielding brace system; the geometric parameters were analyzed by the finite element method, and the effectiveness of the brace with ductile castings in enhancing the energy dissipation capacity and lateral displacement resistance of the frame structure was verified by experiments. In addition, the researchers proposed BRB to replace the ordinary brace and conducted optimization and improvement research on it. The traditional BRBs are generally composed of cross shaped and I-shaped section steel plate and the constraints are composed of concrete filled with steel tube. Wakabayashi (1972) invented the buckling-restrained brace (BRB) and conducted an initial study on it. Fujimoto et al. (1988) developed BRBs with concrete-filled steel tube; mortar filled the space between the inner and outer steel tubes to improve the seismic and energy dissipation capacity. Clark and Kasai (1999) analyzed BRBs' bearing capacity and energy dissipation by experimenting with rectangular and cross sections of the inner tube. Tsai et al. (2004) presented a double-sleeve, double-kernel BRB to reduce the connection length and number of bolts; then, they performed theoretical and experimental analyses. With the gradual application of BRBs, researchers have improved the core cross section, materials and end connection type of BRBs, including perforated core BRB, double-stage yield BRB, all-steel BRB and dual-gusset-plate connections for BRB (Chou et al., 2012; Hoveidae and Rafezy, 2012; Piedrafita et al., 2015; Barbagallo et al., 2019). And the corresponding analysis and design methods have also been gradually applied (Avci-Karatas et al., 2018, 2019). Based on the assembly and replaceable design concept, Guo et al. (2010) designed a new type of assembled BRB to overcome the disadvantage on difficulty of precision control between the inner core and outer contained members due to operation of concrete casting in traditional BRBs, and improve installation efficiency. Steven and Wiebe (2019) proposed an alternative connection that reduces the cost of repair by confining all damage to a replaceable brace module.

On the basis of the excellent mechanical properties and stable energy dissipation performance of the BRB, the author (Yin and Pan, 2018; Yin et al., 2020) developed a new BRB with ductile castings to further improve the overall performance of BRBs and frames, the brittle failure of the gusset plates was solved, and double-stage yield energy dissipation was realized. With changes in the geometric parameters and details of the ductile castings, the inelastic deformation of the structure could be confined to the ductile castings and BRB. Consequently, the energy dissipation performance of the concentrically braced steel frames is improved, structural safety is increased, and the structure can be replaced after earthquakes.

This paper focuses on laboratory tests and finite element analysis of a structure with different design parameters. The length of the yielding segment and width-to-thickness ratio of the ductile castings, and the mechanical properties of structures under loading are studied. The results showed that the energy dissipation capacity of this new steel frame system is stable, and the inelastic behavior is confined to the ductile castings and BRB. It also satisfies the maximum elastic and elastic-plastic drift angles required by the Code for Seismic Design of Buildings (GB 50011-2010, 2016). The conclusion provides a reference for further improvement and engineering application.

2. The Design of the Buckling Restrained Braced Steel Frames with Ductile Castings

2.1 The Design Concept

The BRB steel frames with ductile castings consist of the components shown in Fig. 1. Each component is manufactured

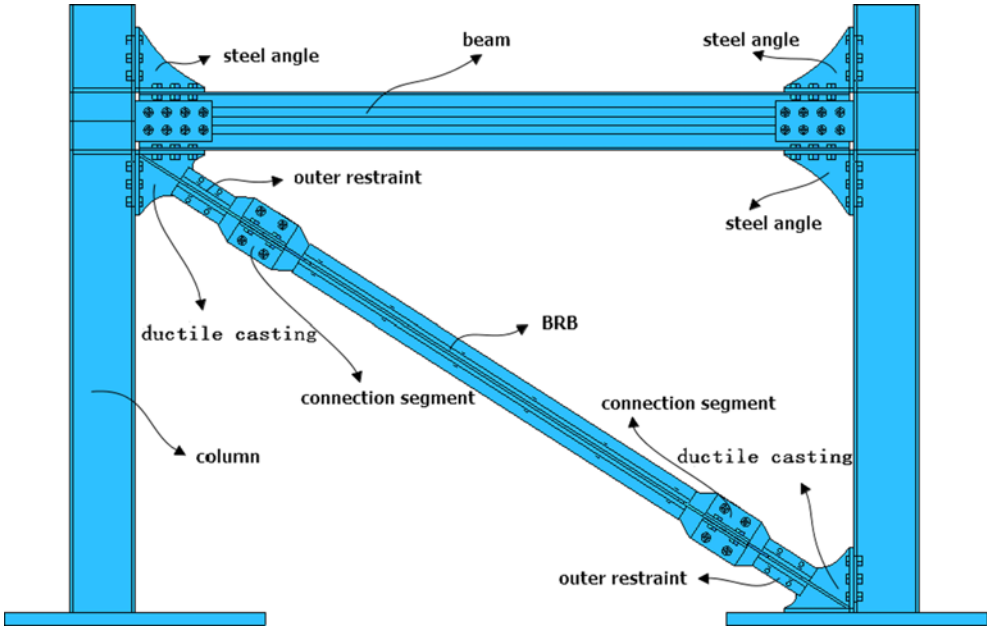

Fig. 1. BRB Steel Frames with Ductile Castings

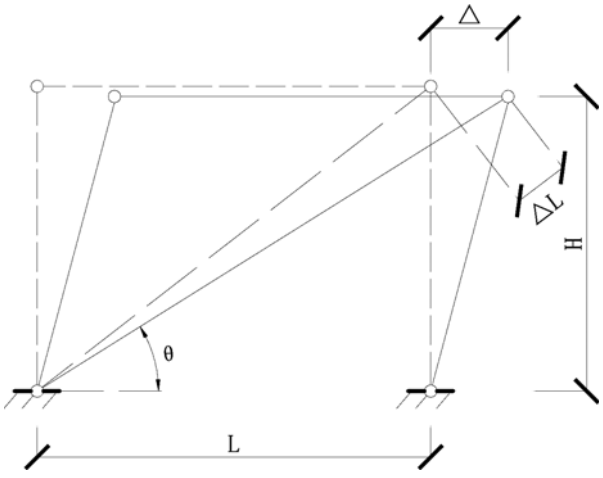

Fig. 2. Schematic of One-Story Structure

in a factory and assembled by bolts at the construction site. The ductile castings at both ends of the BRB can confine the inelastic deformation of the structure to this region. This reduces the stress distribution in the joint field of the beam and the column and avoids brittle failure, forming an assembly structure in which all parts can be replaced.

The lateral stiffness of the structure is provided by the brace and the frame. Therefore, the lateral stiffness ratio is used to design the structure and analyze its seismic performance.

Figure 2 shows a schematic of the concentrically braced frame of a one-story structure. The lateral displacement of the frame under horizontal load is assumed to be slight; therefore, the increment of the angle between the brace and the horizontal line is negligible. The lateral stiffness of the structure is derived as follows.

The axial force of the brace is

$$\Delta L = \Delta\cos\theta = \frac{FL}{EA} \Rightarrow F = \frac{EA\Delta\cos\theta}{L}. \tag{1}$$

Thus, the horizontal component of the brace force is

$$F_x = F\cos\theta = \frac{EA\Delta\cos^2\theta}{L}. \tag{2}$$

The lateral stiffness of the brace is

$$K_B = F_x/\Delta = EA\cos^2\theta\sin\theta/h, \tag{3}$$

where L and H are the width and height of the structure, respectively; E is the Young's modulus of the material; and A is the cross-sectional area of the brace.

The lateral stiffness of the frame can be calculated by the D-value method:

$$K_F = 2a\frac{12E_cI_c}{h^3}, \tag{4}$$

where a is a correction coefficient (derivation in Table 1); E_c and I_c are the Young's modulus and moment of inertia of the column, respectively.

The design of the BRB with ductile castings is based on the stiffness ratio method (Jia et al., 2009; Zhao and Guo, 2010). The lateral stiffness ratio is defined as k:

$$k = K_B/K_F. \tag{5}$$

The lateral stiffness ratio should be between 2 and 5. Then, the sectional area of the brace can be determined:

$$A = k\cdot K_F\cdot h/E\sin\theta\cos^2\theta. \tag{6}$$

The ductile castings and core of the BRB are cross-sectional; they are connected to the frame by bolts. The axial force ratio of the BRB and ductile castings is defined as

Table 1. Calculation Table of Correction Coefficient

Floors	Schematic of structure	Beam–column stiffness ratio K	Correction coefficient α
The ground floor	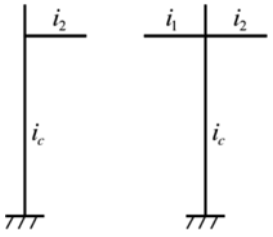	$K=\frac{i_1+i_2}{i_c}$	$\alpha=\frac{0.5+K}{2+K}$
The other floor	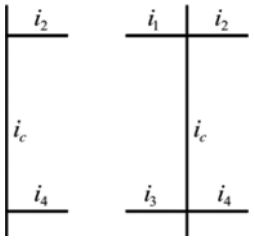	$K=\frac{i_1+i_2+i_3+i_4}{2i_c}$	$\alpha=\frac{K}{2+K}$

Note: i_1, i_2, i_3, i_4 are the linear stiffness of the beam. i_c is the linear stiffness of the column.

$$n = p_B / p_C \,, \tag{7}$$

where p_B is the axial yield load of the BRB. p_c is the axial yield load of the ductile casting.

2.2 Specimen Design

With a nine-story steel frame as a prototype, the structure is designed according to the Standard for Design of Steel Structure (GB 50017-2017, 2017) and Code for Seismic Design of Buildings (GB 50011-2010, 2016). Due to the test conditions, the prototype model was reduced by a scale of 1/3. The column section size is H150 × 150 × 6 × 8, and the beam section size is H135 × 100 × 6 × 6, as shown in Fig. 3.

Two BRB steel frames with ductile castings with 1.18 and 1.08 axial force ratio were designed (named CBRBSF-1 and CBRBSF-2). According to the research group's previous research

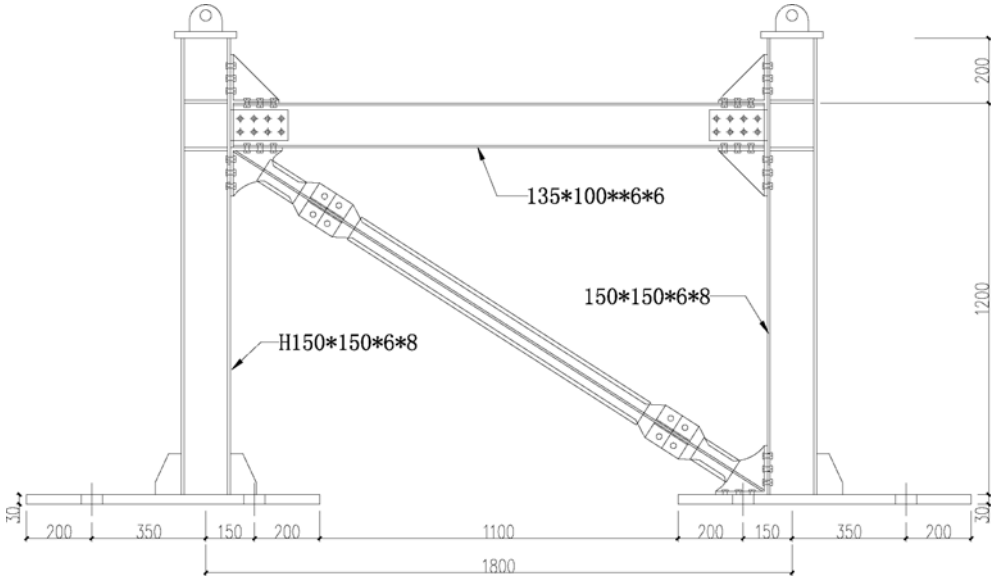

Fig. 3. Buckling Restrained Braced Steel Frames with Ductile Castings

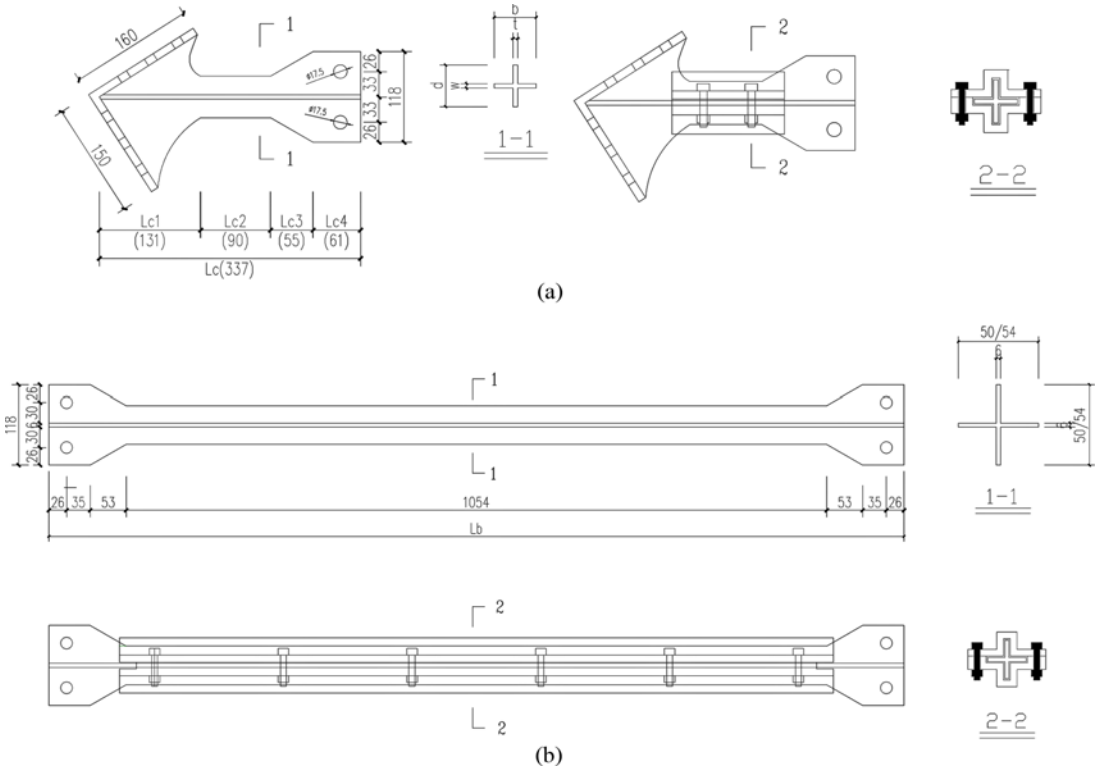

Fig. 4. Schematic of Ductile Casting and BRB: (a) Ductile Casting, (b) BRB

Table 2. Specimen Material Properties

Type	Yield strength *fy*/MPa	Ultimate strength *fu*/MPa	Elastic modulus *E*/MPa	Elongation *δ*/%
Ductile casting	237	424	232,800	26
Core of BRB	240	450	220,000	25
Outer of BRB	242	436	210,500	26
Steel frame	246	438	205,000	24

(Li, 2019), the stiffness and stability of a ductile casting affect the energy dissipation performance of the whole brace, and adding an external restraint to the energy dissipation section of the ductile casting can better resist torsional instability. Therefore, in this test, the outer restraint component was set at the energy dissipation section of the ductile casting. The details and dimensions of the ductile casting and BRB are shown in Fig. 4.

Figure 4 shows the details and dimensions of the ductile

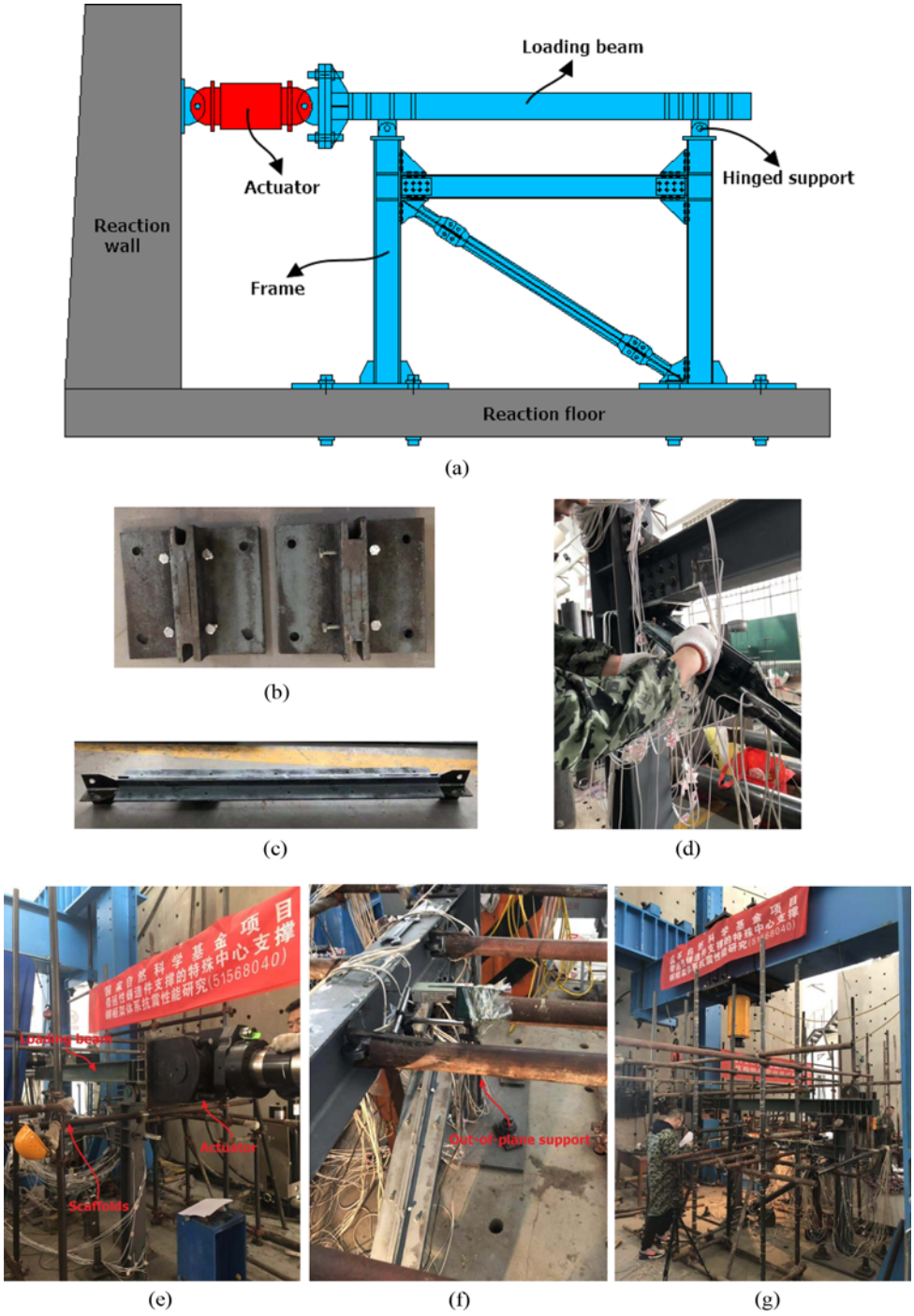

Fig. 5. Experimental Setup: (a) Details of Test Setup, (b) Outer Restraint, (c) BRB, (d) Ductile Casting Assembled, (e) Test Equipment, (f) Scaffolds, (g) Test Preparation

casting and BRB. The total length of the ductile casting is L_c, including the frame–casting interface segment L_{c1}, yielding segment L_{c2}, transition segment L_{c3}, and BRB-casting interface segment L_{c4}. The core of the BRB is a welded cross section, and L_b is the total length of the BRB. The outer restraint component is set in the yielding segment of the ductile casting, which is welded at an unequal steel angle and connected by bolts. This component can restrain the buckling of the yielding segment and ensure the energy dissipation capacity of the ductile casting. In addition, a certain gap length is set at both ends of the outer restraint component to satisfy the requirements of axial deformation.

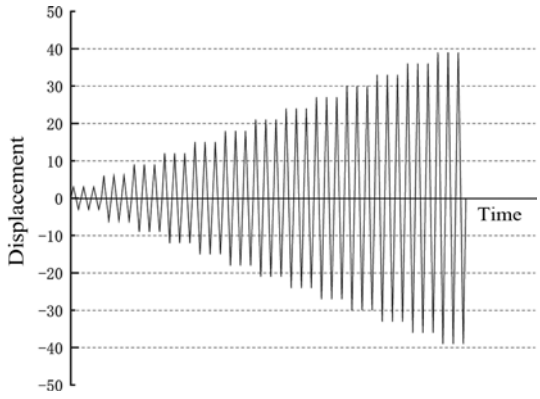

Fig. 6. Loading Protocol

3. Experimental Study of BRB Steel Frames with Ductile Castings

3.1 Material Properties

Table 2 lists the material properties of the steel frame, BRB, and ductile casting, as measured by tensile coupon tests.

3.2 Test Setup and Instrumentation

The experiment was conducted in the structural experiment hall of Lanzhou University of Technology. The loading device adopted the MTS electro-hydraulic servo for an actuator with a maximum output load of 1,000 kN and a maximum range of ±250 mm. After the specimens were assembled, the loading beam was arranged to transfer horizontal force to the steel frame by connecting the lifting lug of the frame with a pin (d = 50 mm). The bottom plate of the specimen and the reaction floor were connected by a screw rod of d = 60 mm, as shown in Fig. 5. The lateral side of the beam was restrained by the steel tube with a roller, and the whole scaffold was installed to ensure the overall stability of the steel frame.

In this research, the displacement loading control was according to the Specification for Seismic Test of Buildings (JGJT 101-2015, 2015). The amplitude of the displacement loading is shown in Fig. 6. Each level was cycled three times. The test would be stopped when the bearing capacity had decreased noticeably and local damage or damage to the whole structure occurred.

3.3 Test Point Layout

All data in the test were collected through a DH3816 static strain acquisition system (Fig. 7(a)). Displacement meters with an accuracy of 0.01 mm were installed at the position shown in Figs. 7(b) and 8(a). The No. 1 and No. 2 displacement meters measured horizontal drift in the plane of the frame. Nos. 3 and 4 measured the axial deformation of the BRB. Nos. 5 to 9 measured the out-of-plane displacement of the ductile casting and BRB. The steel ruler was set at the outer restraint component of the ductile casting to measure the axial deformation. The strain gauge arrangements of the frame, ductile casting, and BRB are

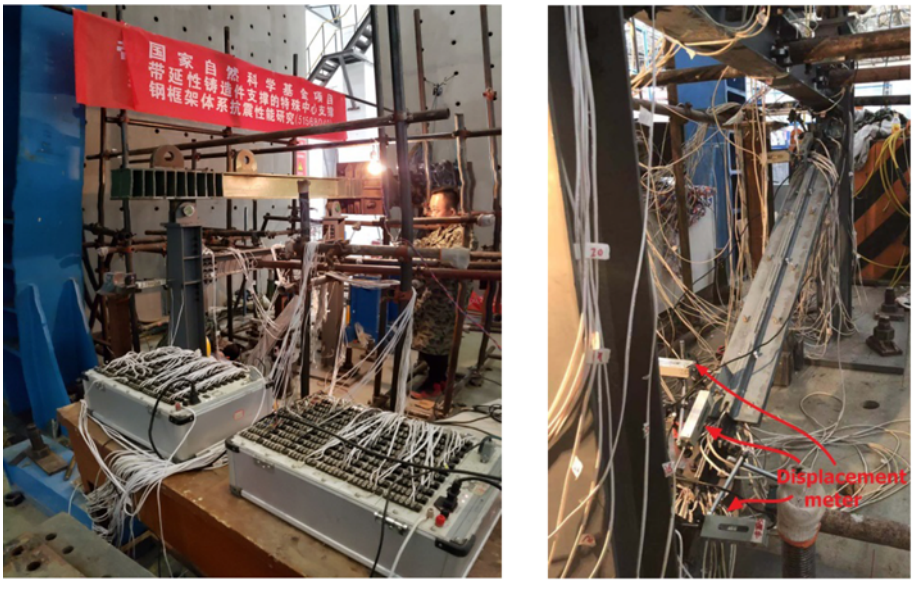

Fig. 7. Data Acquisition Equipment: (a) DH3816, (b) Displacement Meter

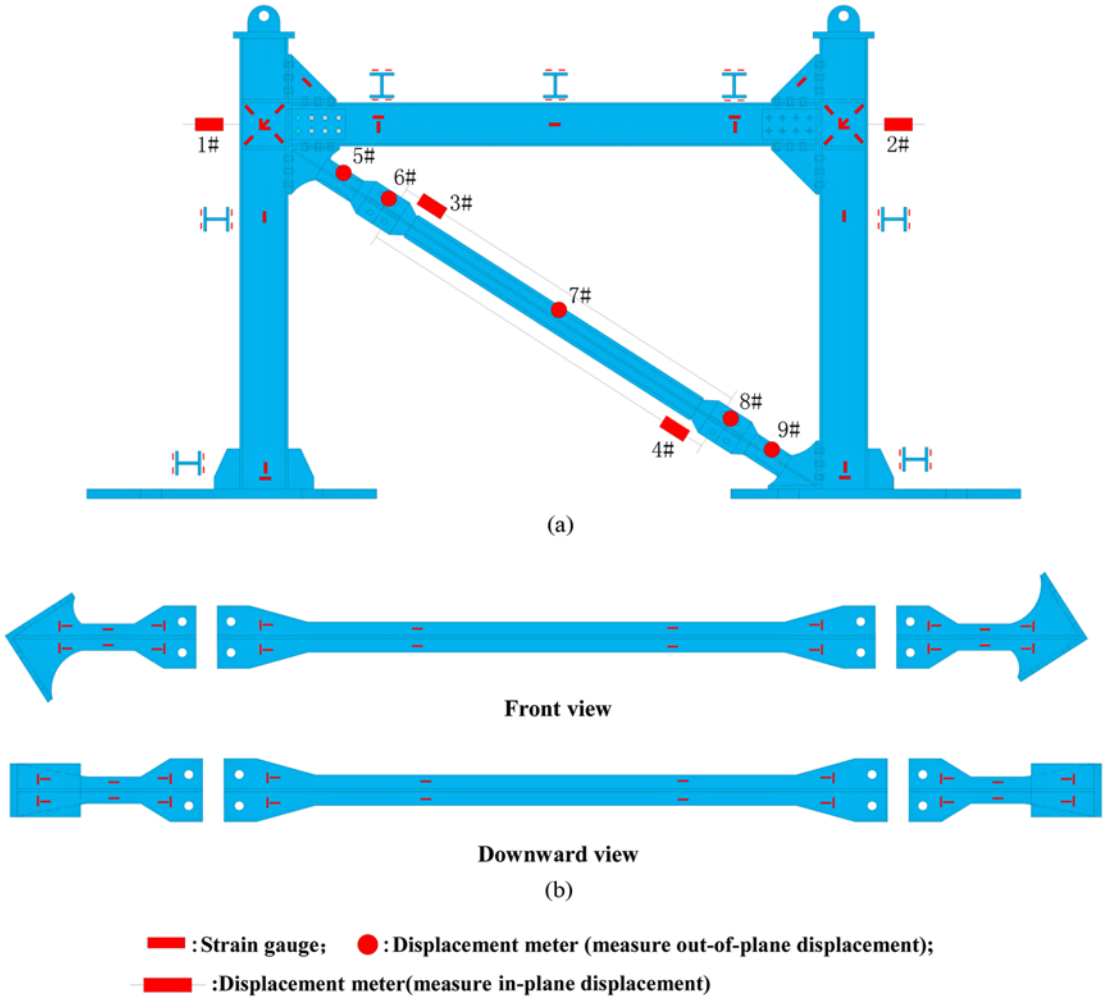

Fig. 8. Measurement Arrangement of Strain Gauge and Displacement Meter: (a) Strain Gauge and Displacement Meter Arrangements of the Frame, (b) Strain Gauge Arrangements of the Ductile Casting and BRB

shown in Fig. 8.

3.4 Experimental Phenomenon

In this paper, the following rules were established. 1) Loading direction: push was positive; pull was negative. 2) The column near the MTS side was marked the No. 1 column, and the ductile casting connected to it was No. 1. The other side was the No. 2 column and No. 2 ductile casting.

CBRBSF-1: Under cyclic loading, when the displacement reached 4.8 mm, there was a slight sliding at the connection between the BRB and ductile casting. When the displacement reached 9 mm under tension, the measured value of the steel ruler at the No. 2 ductile casting changed by 1.5 mm, indicating that the ductile casting had started producing axial deformation. At 12 mm and 15 mm, the casting and core of BRB were twisted and in contact with the restraining member due to the initial imperfection caused by insufficient processing. When the displacement reached 18 mm, the friction sound between the core and the restraining member of the BRB increased, and the beam connected to column No. 1 produced a slight deformation at the bottom flange of its end. When the displacement reached 24 mm, the axial deformations of ductile castings No. 1 and No. 2 and the BRB were 5.5 mm, 5.8 mm, and 2.7 mm, respectively. Therefore, when the maximum inelastic drift angle of 1/50 was reached, the ductile casting bore most of the plastic deformation. When the displacement reached 36 mm, a large out-of-plane deformation occurred at the connection between the ductile casting and BRB. Meanwhile, local buckling occurred at the bottom flange of the left end of the beam (position connected with the ductile casting), the bearing capacity of the specimen began to decline, and the test thus ended.

CBRBSF-2: Before the displacement reached 18 mm, the experimental phenomenon of CBRBSF-2 was basically consistent with that of CBRBSF-1. When the displacement reached 24 mm, the axial deformation value of ductile castings No. 1 and No. 2 and the BRB were 5.5 mm, 5.8 mm, and 2.7 mm, respectively. The deformation trend was consistent with that of CBRBSF-1, which indicated that the ductile casting bore most of the plastic deformation. Continue loaded to 39 mm, the same phenomenon appeared as specimen CBRBSF-1 and the test ended.

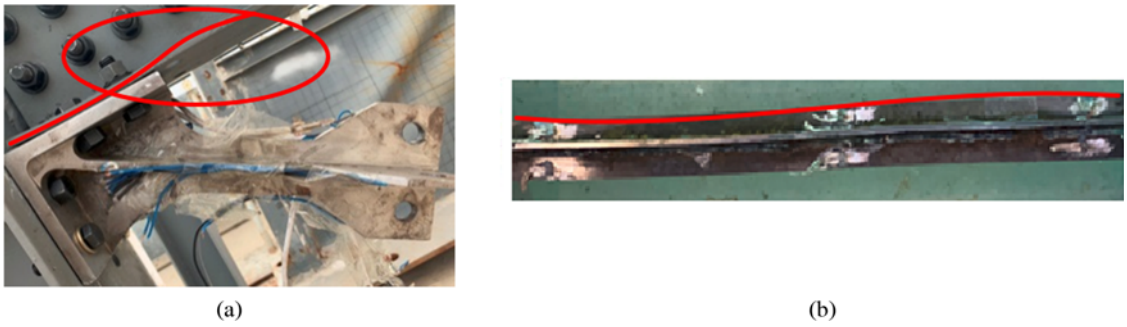

Fig. 9. Failure Mode of Specimen: (a) Bottom Flange Buckling at End of Beam, (b) Buckling at Core of BRB

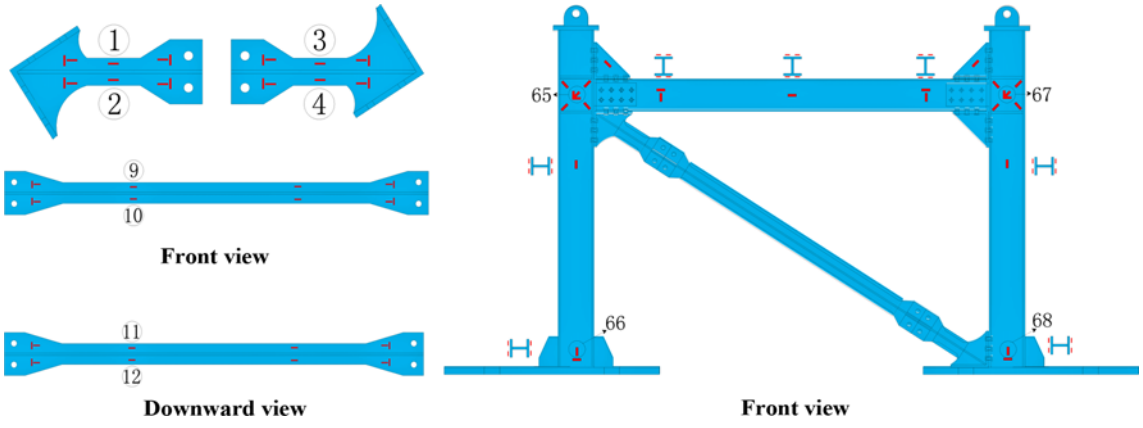

Fig. 10. Measurement Number of Strain Gauge in Ductile Casting, Core of BRB and Frame

3.5 Failure Mode

The yield mode and failure characteristics of the two specimens were basically same. Under cyclic loading, when the lateral displacement reached 4.8 mm (1/250 limit value of the elastic drift angle), the whole frame and brace remained elastic. When the displacement increased to 12 mm (H/100), the tensile and compressive deformations of the ductile casting exceeded the elastic stage, and it was the first to enter the elastic-plastic stage for yield energy dissipation. As the displacement approached 24 mm (H/50), the core of the BRB yielded to dissipate energy, the displacement continued to increase and exceeded the limit of the inelastic (elastic-plastic) drift angle of 1/50. When the displacement reached 36 mm, the bottom flange of the left end of the steel beam connected to column No. 1 showed local buckling. Fig. 9(a) shows the bottom flange buckling at the end of the beam. Fig. 9(b) shows the failure characteristics of the high-order buckling deformation of the core of the BRB. Finally, under the action of cyclic tension and compression, the BRB with ductile castings showed excessive deformation, the bearing capacity began to decline, and the experiment stopped. In the whole process, there was no obvious deformation in the joint field and the column foot of the frame. The test indicated that the failure mode of two specimens were ductile failure.

3.6 Stress Analysis

The stress change of the main members in the BRB steel frame with ductile castings was studied. The measurement number of strain gauge in ductile casting, core of BRB and frame is shown in Fig. 10. And the strain data of the ductile casting, BRB, joint field, and the column foot of the frame were analyzed when the frame story drift was 12 mm, 15 mm, 18 mm, 24 mm, 33 mm, and 39 mm.

As shown in Fig. 11(a), when the lateral displacement reaches 4.8 mm (H/250), the measured stress value at the brace and frame of CBRBSF-1 was small. When the displacement reached 12 mm (H/100), the stress at points No. 1 to No. 4 of the ductile casting was 224.2 MPa, 216.1 MPa, 221.4 MPa, and 225.6 MPa, which were close to the yield stress. Therefore, the ductile casting was the first member to dissipate energy. At this time, the maximum stress value at points No. 9 to No. 12 of the core of the BRB was only 188.4 MPa, which still maintained the elastic state. With the increase in displacement, the stress values of the ductile casting and core of the BRB increased gradually. When the displacement reached 24 mm (H/50), the stress at points No. 1 to No. 4 were 271.6 MPa, 278.4 MPa, 288.6 MPa, and 281.2 MPa. The maximum stress value at points No. 9 to No. 12 was 256.8 MPa. Therefore, when the displacement reached the limiting value of the elastic-plastic story drift, both the ductile casting and the BRB entered the plastic state and dissipated energy together. As indicated by the curves divided by a red broken line in Fig. 11, the stress of the ductile casting (measuring points No. 1 to No. 4) was always greater than the stress of the BRB (measuring points No. 9 to No. 12).

During the whole loading process, the joint field of the beam–

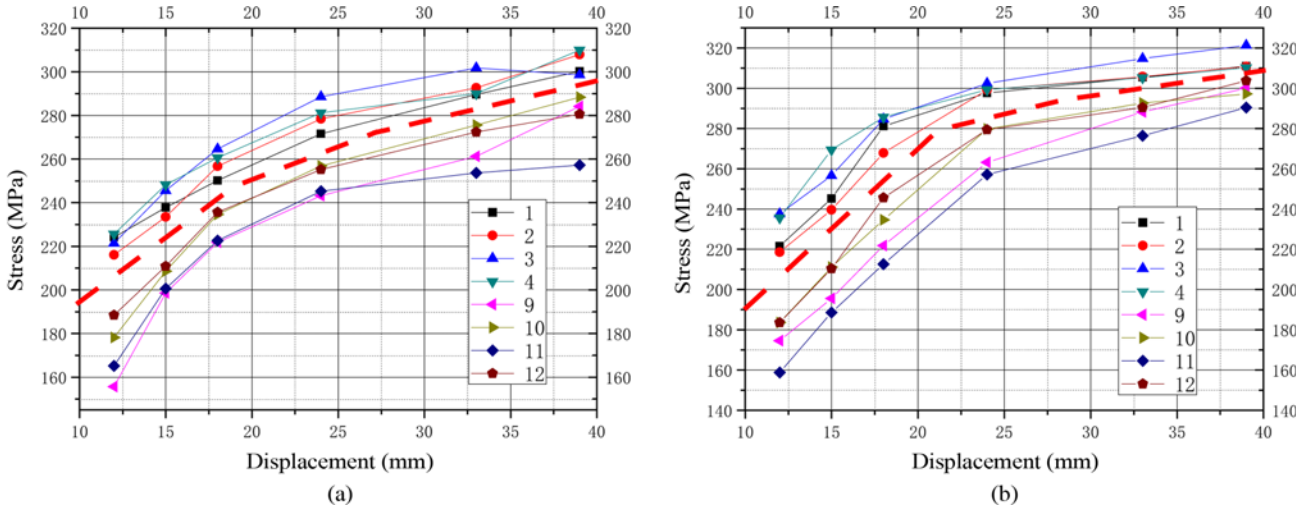

Fig. 11. Comparison of Stress Values of Ductile Casting and BRB: (a) CBRBSF-1, (b) CBRBSF-2

Table 3. Stress Values of Joint Field and Column Foot (MPa)

	Measuring point	Displacement (mm)					
		12	15	18	24	33	39
Joint field and column foot (CBRBSF-1)	65	84.2	120.2	140.2	162.4	201.6	200.8
	66	101.2	129.8	142.8	185.2	210.4	243.9
	67	88.6	111.4	120.6	125.4	160.8	183.2
	68	106.1	133.5	146.7	188.4	212.7	247.9
Joint field and column foot (CBRBSF-2)	65	95.4	124.6	147.2	173.8	212.8	234.2
	66	104.6	135.7	166.2	193.6	236.2	243.7
	67	110.4	120.6	187.4	197.8	210.6	223.9
	68	101.2	123.6	153.7	184.6	223.2	240.5

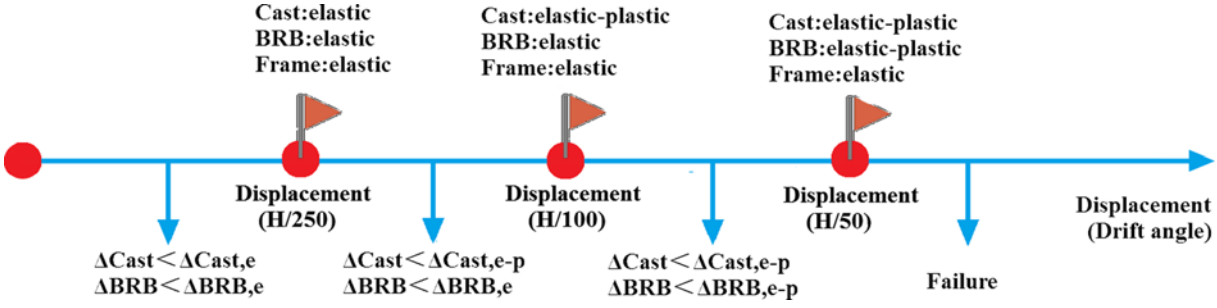

Fig. 12. Two-Stage Energy Dissipation Design Concept

column and the column foot of the frame remained in the elastic state. When the maximum lateral displacement was reached, their stress values became only 200.8 MPa and 247.9 MPa, respectively, as shown in Table 3. Similarly, the same rule can be found from the stress analysis of CBRBSF-2, as shown in Fig. 11(b) and Table 3. The above results show that the ductile casting entered the plastic state before BRB, and BRB supplemented the energy dissipation; this finding conforms to the two-stage energy dissipation design concept (Fig. 12).

3.7 Hysteretic Performance

Under cyclic loading, the energy dissipation capacity of the structure can be reflected by the energy dissipation coefficient E. These can be calculated according to the following equations:

$$E = \frac{S_{ABC+CDA}}{S_{\Delta OBE+\Delta ODF}}, \tag{8}$$

where $S_{ABC+CDA}$ is the area enclosed by the hysteresis loop. $S_{\Delta OBE+\Delta ODF}$ is the sum of the areas of $\Delta OBE$and ΔODF. Fig. 13 shows the calculation.

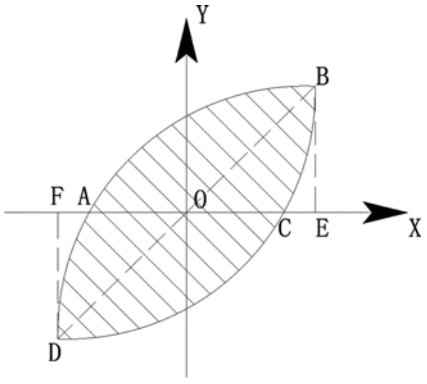

Fig. 13. Calculation Diagram of Energy Dissipation Coefficient *E*

The hysteretic curve of CBRBSF-1 and CBRBSF-2 are shown in Fig. 14. The following conclusions can be derived from the Figs. 13 and 14.

1. During the loading process, the hysteretic curve displayed a spindle shape and was relatively full. The bearing capacity and stiffness did not degrade significantly, and the structure had good plastic deformation that satisfied the 1/50 maximum elastic-plastic drift angle set by the Code for Seismic Design of Buildings (GB 50011-2010).
2. When CBRBSF-1 and CBRBSF-2 were loaded to 36 mm (H/33), a large out-of-plane displacement occurred at the connection between the BRB and ductile casting during the compression process, and the bearing capacity reached the peak value. With continued loading, the bearing capacity and stiffness began to decline. The energy dissipation coefficient of CBRBSF-1 and CBRBSF-2 were 2.03 and 2.09, respectively, which indicated good energy dissipation capacity.

3.8 Skeleton Curve and Stiffness Analysis

The skeleton curve mainly reflects the bearing capacity and stiffness characteristics of a structure. The skeleton curves of two specimens are shown in Fig. 15.

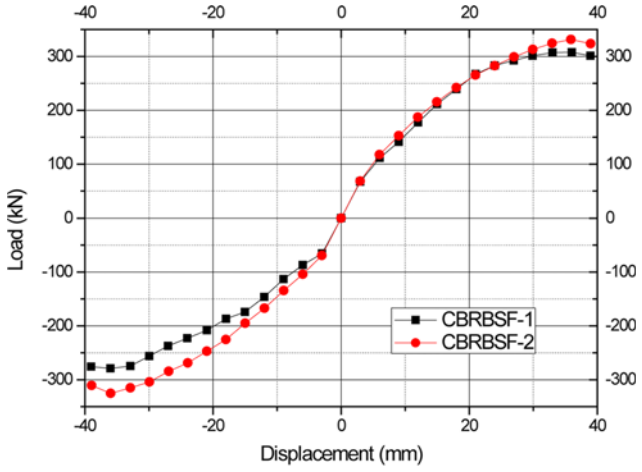

Fig. 15. Comparison of Skeleton Curves

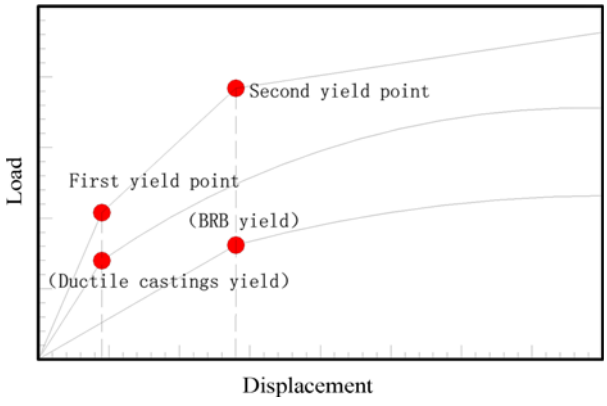

Fig. 16. Trilinear Mechanical Model

1. Under cyclic loading, the skeleton curve of the specimen included elastic, strengthening, and plastic sections. The yield displacement of CBRBSF-1 was 4.82 mm, the corresponding yield load was 109.68 kN, and the initial stiffness was

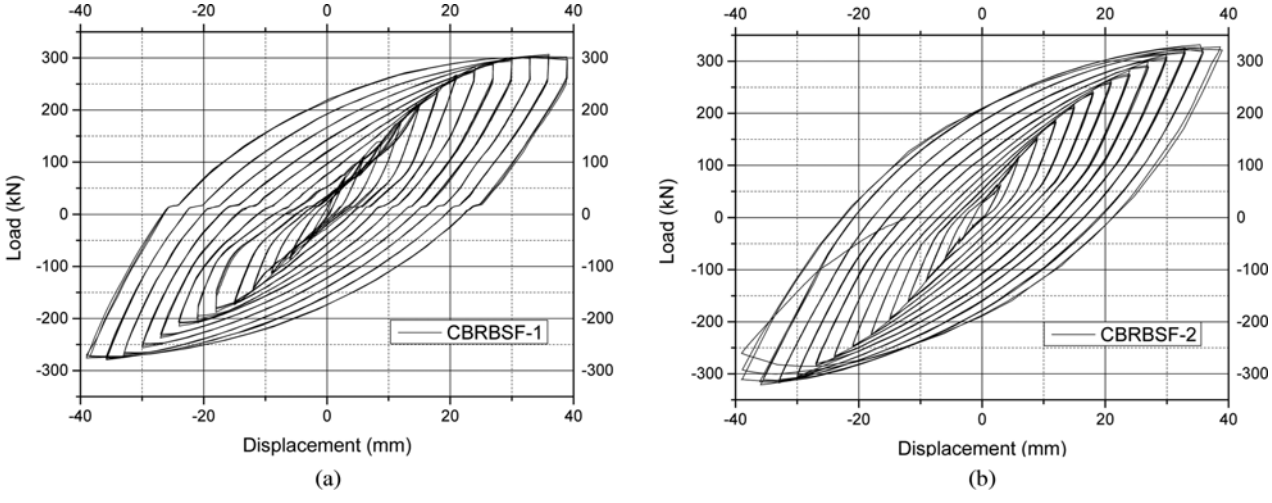

Fig. 14. Hysteretic Curves of CBRBSF-1 and CBRBSF-1: (a) CBRBSF-1, (b) CBRBSF-2

22.76 kN/mm. Upon loading into the first compression cycle of 36 mm, the bearing capacity reached a peak of 307.79 kN, the stiffness degraded to 8.55 kN/mm, and the degradation amplitude was 63.10%.

2. The initial stiffness and bearing capacity of CBRBSF-2 were higher than that of CBRBSF-1. Compared with CBRBSF-1, the ultimate tension and compression bearing capacity of CBRBSF-2 was 331.55 kN and -325.62 kN, which increased by 7.72% and 16.65%, respectively. Moreover, the curves had obvious symmetry in tension and compression, it indicating that the ultimate bearing capacity of specimens could be improved to a certain extent by reducing the axial force ratio of brace.
3. The relationship between the story drift and bearing capacity of the BRB steel frames with ductile castings can be described by a simplified trilinear mechanical model, as shown in Fig. 16. The first point is the yield of the ductile casting, and the second point is the yield of the BRB. When the drift angle was less than 1/250, the ductile casting dissipated energy before the BRB and steel frame. When the drift angle was greater than 1/250 and less than 1/50, both the ductile casting and BRB entered the plastic stage and dissipated energy together. When the drift angle was greater than 1/50, parts of the steel frame yielded and participated in energy dissipation.

4. Finite Element Analysis

4.1 Finite Element Modeling

The finite element models were established using the software ABAQUS. Considering material and geometric nonlinearities, the Standard module was selected for the complete analysis, and initial imperfection and residual stress were ignored. The isotropic and multi-linear kinematic hardening rule was used to verify the elastic and plastic behavior of the specimen respectively. The material properties were obtained from the unidirectional tensile coupon tests in Table 2 and referred to the author's previous tests (2020). Fig. 17 shows the finite element model meshing densities. The contact relationship between the components was set as surface-to-surface contact. The eight-node hexahedron quadratic reduction integral element (C3D8R) was used for the model. To get the refined mesh density and high computational efficiency, the finite element sizes of the column, beam, core of BRB, and other components were 10 mm, 10 mm, 15 mm, and 20 mm, respectively. And a local small element size 5 mm was used in the ductile casting. Besides, in the prior tests, four 6 mm-thick angle plates with four holes for bolted connections was connected to the ductile castings and the BRB ends, for easy replacement of the specimens. In the numerical models, a simplified connection (without holes or bolts) between the ductile castings and BRB end to simulate such a connection detail. Fig. 18 shows the boundary conditions of the finite element models. Translational and rotational degrees of freedom of the bottom-end of both columns and out-of-plane translational degrees of freedom of the frame were restrained. And the horizontal cyclic displacement loading that used in Fig. 6 was applied at the RP-1 reference point on the left side of the frame.

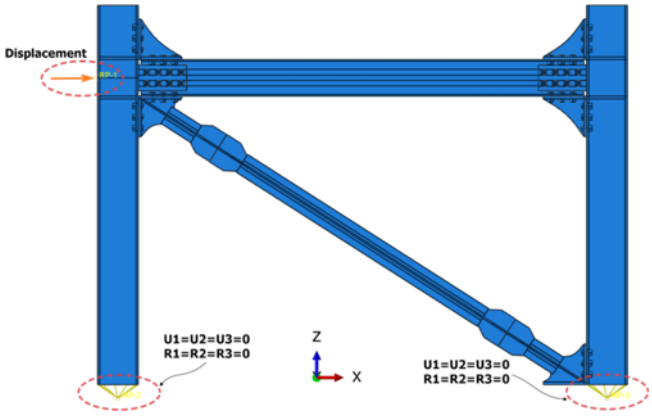

Fig. 18. Boundary Conditions of Finite Element Model

4.2 Verification of Finite Element Models

In the finite element simulation, the deformation of the ductile casting was mainly concentrated on the yielding segment. Under cyclic loading, the yielding segment of ductile casting was the first to enter the elastic-plastic stage for yield energy dissipation. With the increase of displacement, the deformation of yielding segment increased and buckling occurred, as showed in Fig. 19(a). In the test, the deformation and local buckling were also mainly occurred at the yielding segment of ductile casting, as showed in Fig. 19(b).

The deformation and stress distribution mode of finite element

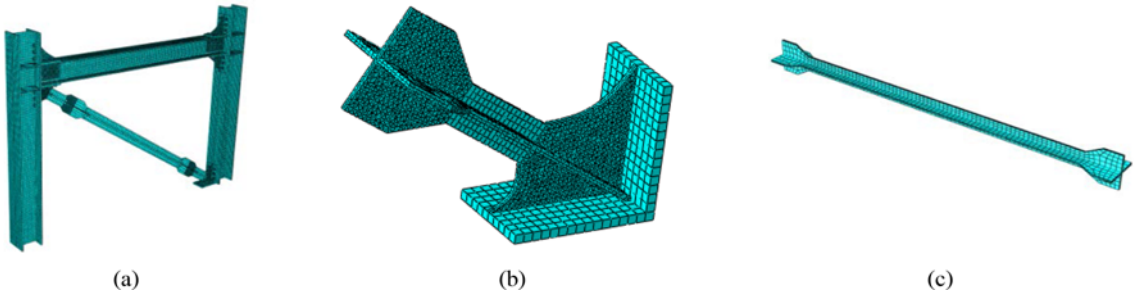

Fig. 17. Finite Element Model: (a) Frame, (b) Ductile Casting, (c) Core of BRB

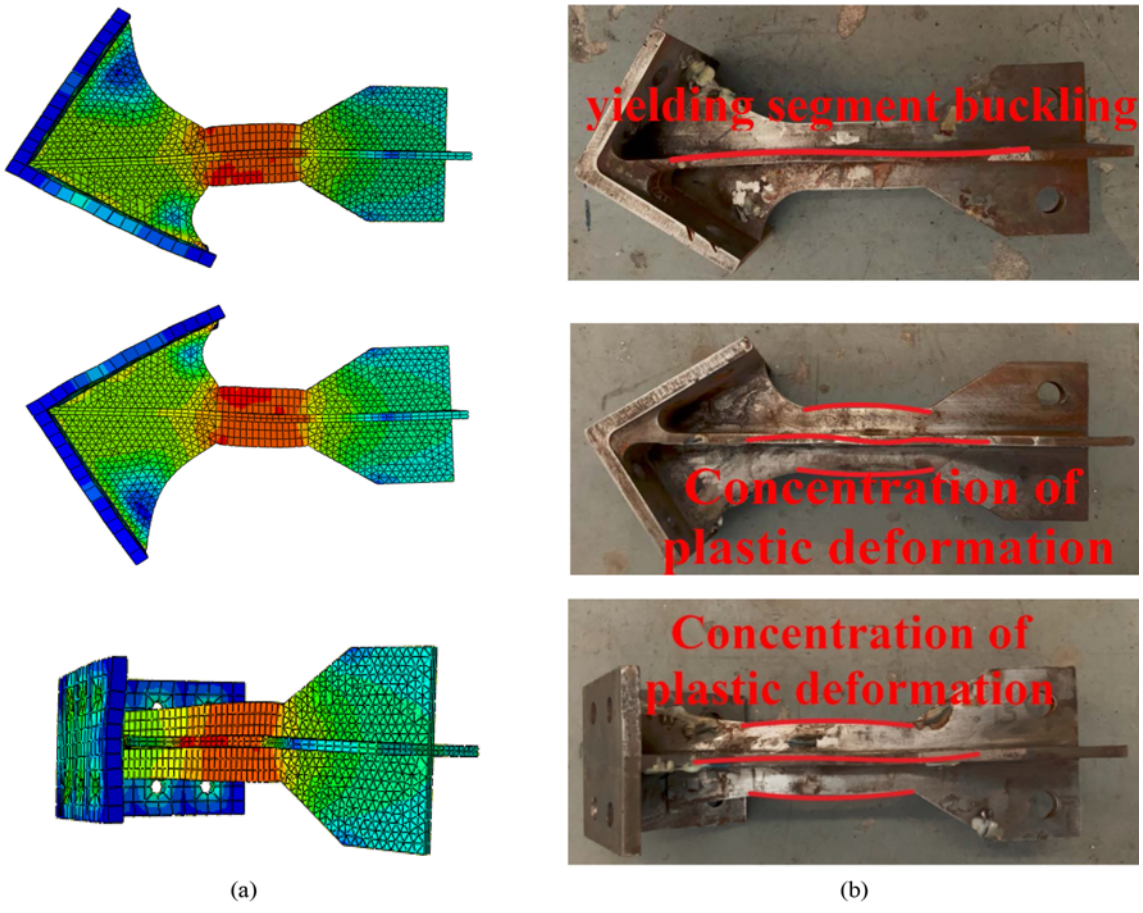

Fig. 19. Test and Finite Element Deformation Comparison Diagram: (a) Finite Element, (b) Test

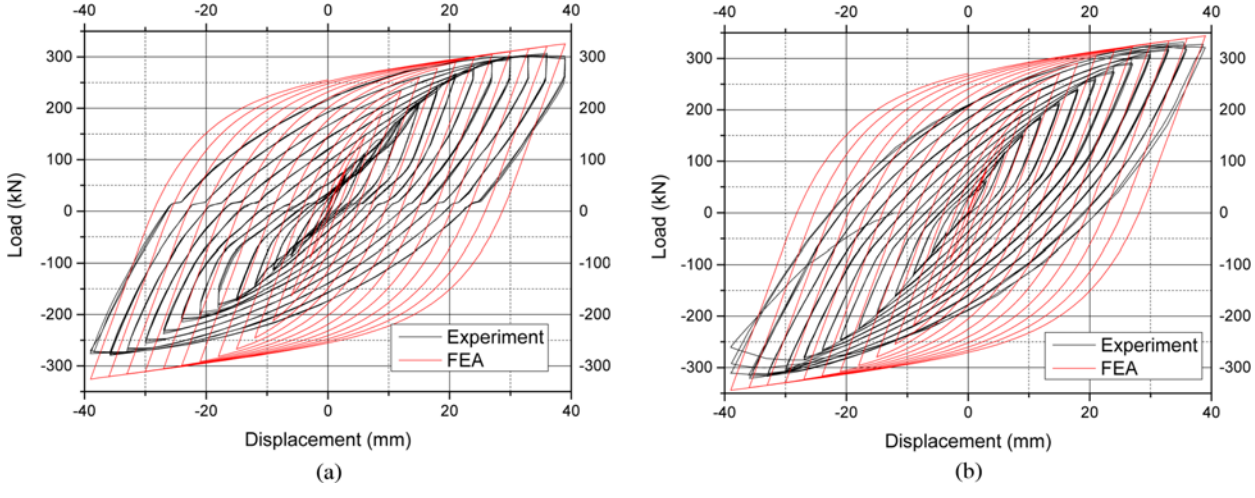

Fig. 20. Comparison of Hysteretic Curves of CBRBSF -1 and CBRBSF -2: (a) CBRBSF-1, (b) CBRBSF-2

simulation was basically consistent with test results. The uniformity of finite element simulation and test results was fully proved.

4.3 Comparison of Hysteretic Performance

As shown in Fig. 20, the hysteresis curve of the finite element analysis was fuller and had a shuttle-like shape. The plastic deformation ability was better than the experimental results. When the ductile castings and core of the BRB began to yield successively under cyclic load, the hysteretic curve bended, the area of the hysteretic loop increased, and the stiffness of the structure slightly decreased. With the increasing load, the deformation of the ductile casting and core of the BRB continuously increased, the hysteresis loop tended to be full and stable, and the maximum hysteresis loop area was large and did not show

Table 4. Comparison of Finite Element and Experimental Results

		Forward loading		Reverse loading	
		K_0 (kN/mm)	P_{max} (kN)	K_0 kN/mm)	P_{max} (kN)
CBRBSF-1	Experiment	22.76	307.79	21.83	-279.20
	Finite element	24.12	325.61	23.92	-325.65
	Difference	5.66%	5.47%	8.74%	5.78%
CBRBSF-2	Experiment	23.19	324.42	22.92	-325.62
	Finite element	25.74	344.31	25.41	-344.37
	Difference	9.91%	5.78%	9.79%	5.44%

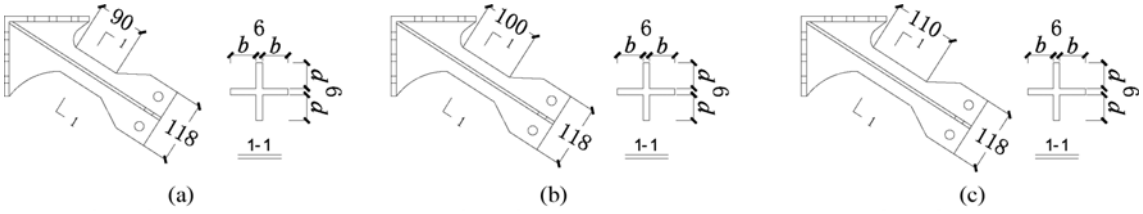

Fig. 21. Models for Parametric Study: (a) CBRBSF-1 – 6, 19, 20, (b) CBRBSF-7 – 12, 21, 22, (c) CBRBSF-13 – 18

pinching. The energy dissipation coefficients obtained by the experiment and finite element were both greater than 2.0, which indicates that the BRB steel frames with ductile castings had strong plastic deformation capacity and good energy dissipation. However, the energy dissipation factor in the test was smaller than that of the finite element due to limitations in the test conditions, such as unsatisfactory constraint and the gap at the bottom of the specimen.

4.4 Comparison of Skeleton Curves

Table 4 show the comparison results of the skeleton curve, initial stiffness (K_0), and peak load (P_{max}) of the test and the finite element. As can be seen from Table 4, the overall fitting degree of the skeleton curve of the test and the finite element was good. Although the finite element and test results show that the BRB steel frames with ductile castings had a higher initial stiffness, there was a certain degree of difference between the test and the finite element. The result of the positive and negative loading test was lower than that of the finite element. The main reason for these findings was that there was a certain installation gap between the specimen, the loading beam, and the reaction floor, which led to slipping of the specimen during the loading process. Moreover, due to the initial imperfection caused by the processing of the specimen, out-of-plane displacement of the brace occurred during the test. Consequently, the load and displacement data obtained by the test were smaller than those of the finite element analysis. At the late stage of loading, the two curves still showed the same variation trend. The differences of initial stiffness and peak loads between the test and the finite element were less than 10%. These differences can be controlled within the acceptable range of engineering if the accidental factors in the test process were removed.

5. Parametric Analysis of BRB Steel Frames with Ductile Castings

5.1 Analysis Parameter

The influence of geometry parameters on the stress distribution mode and mechanical properties of the BRB steel frames with ductile castings was investigated using ABAQUS. Twenty-two models with different axial force ratios of BRB and ductile casting, length of yielding segment, and width-to-thickness ratio of the ductile casting were designed, as shown in Fig. 21 and Table 5. Ductile casting thickness is 6 mm. Axial force ratios of BRB and ductile casting were 0.87, 0.92, 1.00, 1.08, 1.18 and 1.28. Lengths of yielding segment L_{c2} of ductile casting were 90, 100 and 110. Width-to-thickness ratios of the ductile casting were 7.7, 8.3, 9, 9.7, 10.3 and 11.

5.2 Stress Distribution

Under the action of cyclic loading, the overall stress distribution law of buckling-restrained braced steel frames with ductile castings with different parameters is basically consistent. At the initial stage of loading, ductile castings enter the yield stage before BRB. As the loading progresses, both of ductile castings and BRB enter into the yield stage and dissipated energy together. It can be concluded from the analysis that the maximum stress of the structure is mainly concentrated in ductile castings, while the stress at joint field of the beam–column is relatively small. As shown in Fig. 22 and Table 6, the maximum stress of ductile castings in CBRBSF-1 was 349.0 MPa, and the maximum stress at joint field of the beam–column was 305.5 Mpa. However, for BRBSF without ductile casting, the stress of gusset plate is 320.2 Mpa, and the joint field of the beam–column stress is up to 357.5 Mpa. From the above data, it can be concluded that a large amount of plastic deformation can be concentrated in ductile

Table 5. Geometry Parameters of BRB and Ductile Casting

Geometry parameters of BRB				Geometry parameters of ductile casting/ mm							
Number	Length of the yielding core/mm	Section of the yielding core/mm	n	L_{c1}	L_{c2}	L_{c3}	L_{c4}	t	w	b	d
CBRBSF-1	1,054	58 × 6	1.28	131	90	55	61	6	6	46	46
CBRBSF-2	1,054	58 × 6	1.18	131	90	55	61	6	6	50	50
CBRBSF-3	1,054	58 × 6	1.08	131	90	55	61	6	6	54	54
CBRBSF-4	1,054	58 × 6	1.00	131	90	55	61	6	6	58	58
CBRBSF-5	1,054	58 × 6	0.93	131	90	55	61	6	6	62	62
CBRBSF-6	1,054	58 × 6	0.87	131	90	55	61	6	6	66	66
CBRBSF-7	1,034	58 × 6	1.28	131	100	55	61	6	6	46	46
CBRBSF-8	1,034	58 × 6	1.18	131	100	55	61	6	6	50	50
CBRBSF-9	1,034	58 × 6	1.08	131	100	55	61	6	6	54	54
CBRBSF-10	1,034	58 × 6	1.00	131	100	55	61	6	6	58	58
CBRBSF-11	1,034	58 × 6	0.93	131	100	55	61	6	6	62	62
CBRBSF-12	1,034	58 × 6	0.87	131	100	55	61	6	6	66	66
CBRBSF-13	1,014	58 × 6	1.28	131	110	55	61	6	6	46	46
CBRBSF-14	1,014	58 × 6	1.18	131	110	55	61	6	6	50	50
CBRBSF-15	1,014	58 × 6	1.08	131	110	55	61	6	6	54	54
CBRBSF-16	1,014	58 × 6	1.00	131	110	55	61	6	6	58	58
CBRBSF-17	1,014	58 × 6	0.93	131	110	55	61	6	6	62	62
CBRBSF-18	1,014	58 × 6	0.87	131	110	55	61	6	6	66	66
CBRBSF-19	1,054	52.5 × 6	1.08	131	90	55	61	6	6	50	54
CBRBSF-20	1,054	47 × 6	1.08	131	90	55	61	6	6	46	54
CBRBSF-21	1,034	52.5 × 6	1.08	131	100	55	61	6	6	50	54
CBRBSF-22	1,034	47 × 6	1.08	131	100	55	61	6	6	46	54
BRBSF	1,054	58 × 6	/	/							

Note: CBRBSF is buckling-restrained braced steel frames with ductile castings. BRBSF is buckling-restrained braced steel frames.

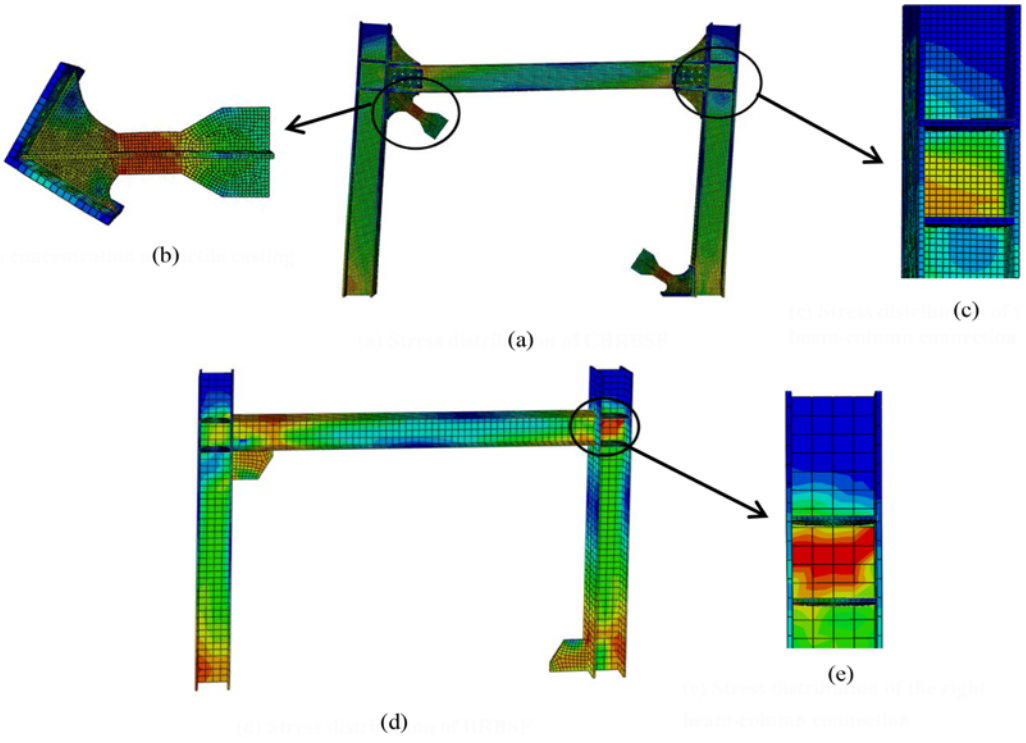

Fig. 22. Stress Distribution of the CBRBSF and BRBSF at Maximum Lateral Displacement: (a) Stress Distribution of CBRBSF, (b) Stress Concentration at Ductile Casting, (c) Stress Distribution of the Right Beam-Column Connection, (d) Stress Distribution of BRBSF

Table 6. Maximum Stress Value of the CBRBSF and BRBSF

Number	Maximum stress/MPa		Ductility	Number	Maximum stress/MPa		Ductility
	Ductile casting/ gusset plate	Joint field of the beam–column			Ductile casting/ gusset plate	Joint field of the beam–column	
CBRBSF-1	349.0	305.5	4.86	CBRBSF-13	270.8	296.7	4.87
CBRBSF-2	372.4	286.7	4.99	CBRBSF-14	295.9	305.1	5.06
CBRBSF-3	399.7	265.8	5.07	CBRBSF-15	315.5	300.8	5.19
CBRBSF-4	398.7	268.3	6.16	CBRBSF-16	320.5	295.2	6.17
CBRBSF-5	389.2	280.3	6.15	CBRBSF-17	313.6	305.6	6.16
CBRBSF-6	379.3	298.7	6.17	CBRBSF-18	301.7	311.5	6.15
CBRBSF-7	318.1	310.6	4.82	CBRBSF-19	407.7	285.8	4.97
CBRBSF-8	332.4	303.2	5.09	CBRBSF-20	402.6	279.4	4.82
CBRBSF-9	350.9	294.2	5.19	CBRBSF-21	368.2	302.3	5.09
CBRBSF-10	385.7	268.6	6.15	CBRBSF-22	360.3	299.2	4.90
CBRBSF-11	382.3	269.3	6.14	BRBSF	350.2	381.7	4.52
CBRBSF-12	370.2	280.2	6.16				

Table 7. Energy Dissipation Coefficient and Equivalent Viscous Damping Coefficient

Number	CBRBSF-1	CBRBSF-2	CBRBSF-3	CBRBSF-4	CBRBSF-5	CBRBSF-6	CBRBSF-7	CBRBSF-8
E	2.130	2.289	2.314	2.274	2.257	2.248	2.284	2.297
ξ_{eq}	0.339	0.364	0.368	0.362	0.359	0.358	0.364	0.366
Number	CBRBSF-9	CBRBSF-10	CBRBSF-11	CBRBSF-12	CBRBSF-13	CBRBSF-14	CBRBSF-15	CBRBSF-16
E	2.327	2.261	2.248	2.231	2.174	2.279	2.321	2.264
ξ_{eq}	0.370	0.359	0.358	0.355	0.346	0.363	0.369	0.360
Number	CBRBSF-17	CBRBSF-18	CBRBSF-19	CBRBSF-20	CBRBSF-21	CBRBSF-22	BRBSF	
E	2.247	2.228	2.306	2.299	2.324	2.318	2.011	
ξ_{eq}	0.358	0.355	0.367	0.366	0.369	0.368	0.320	

Note: E and ξ_{eq} are energy dissipation coefficient and equivalent viscous damping coefficient of CBRBSF.

castings through the reasonable design, which alleviates the stress in the joint field of beam-column to a great extent. In addition, it can avoid the brittle fracture of the gusset plate due to excessive weld stress, which affects the performance of the structure.

5.3 Ductility

The ductility ratio of buckling-restrained braced steel frames with ductile castings with different parameters is close to each other (Table 6). The structure shows good ductility and the values are all greater than 4. However, the ductility ratio of buckling-restrained braced steel frames with gusset plates is relatively lower than that of steel frames with ductile castings, which indicating that the ductility of the structure is improved by replacing the gusset plates with ductile castings.

5.4 Energy Dissipation Performance

The hysteretic curves of each model displayed a full shuttle-like shape without pinching behavior. The tension and compression capacities of the curve had a symmetrical distribution. Hence, the structure had good balance between tension and compression and strong capacities in terms of plastic deformation and energy dissipation. The energy dissipation coefficient of each model was between 2.1 and 2.4, and the maximum equivalent viscous damping coefficient was 0.37 (Table 7). Thus, the structure had good energy dissipation performance and can dissipate a large amount of energy under an earthquake.

5.4.1 Axial Force Ratio

The axial force ratio has a significant influence on the energy dissipation performance of the structure. A comparison of CBRBSF-1 to CBRBSF-6 shows that the hysteretic curve changed little when the axial force ratio of the BRB and casting was less than or equal to 1 (As shown in Fig. 23). The peak loadings of CBRBSF-3 to CBRBSF-6 were around 370 kN. With the increase in the axial force ratio, the peak loading of the hysteretic curve decreased to 280 kN. Besides, the energy dissipation coefficient varied with the axial force ratio, the energy dissipation coefficient was the largest when the value of axial force ratio was close to 1. Thus, the axial force should be designed within a certain range such that the structure can have a high bearing capacity and good

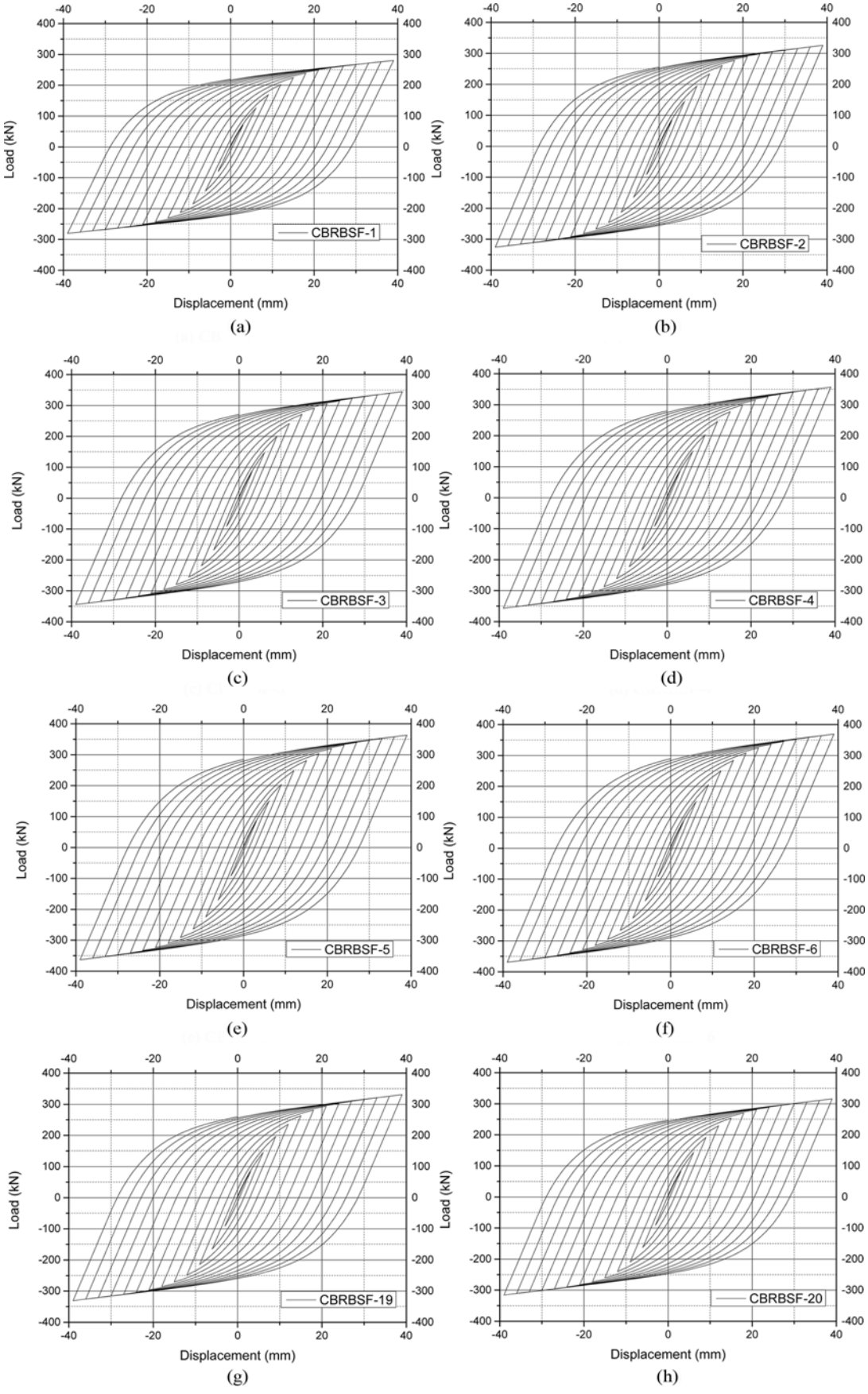

Fig. 23. Hysteretic Curves: (a) CBRBSF-1, (b) CBRBSF-2, (c) CBRBSF-3, (d) CBRBSF-4, (e) CBRBSF-5, (f) CBRBSF-6, (g) CBRBSF-19, (h) CBRBSF-20

energy dissipation capacity at the same time. Therefore, the value of the axial force ratio is suggested to be 0.87 – 1.08.

5.4.2 Lengths of Yielding Segment

Comparisons of CBRBSF-2 and CBRBSF-8 with CBRBSF-14, and CBRBSF-3 and CBRBSF-9 with CBRBSF-15 reveal that the bearing capacity of each model did not change significantly with the increase in the length of the yielding segment from 90 mm to 110 mm. The main reason is that the outer restraint components were set in the yielding segment of the ductile casting. The restraint effect was evident and can prevent any decrease in the bearing capacity of the casting due to local buckling.

5.4.3 Width-to-Thickness Ratio

A comparison of CBRBSF-3 and CBRBSF-19 with CBRBSF-20 shows that the yield bearing capacity and ultimate bearing capacity of the specimens gradually increases with the increase of width-to-thickness ratio of the stiffeners on both sides of the ductile castings. However, with the increase in the width-to-thickness ratio, the amplitude of increase of the bearing capacity gradually decreased (A comparison of CBRBSF-9, CBRBSF-21, and CBRBSF-22 shows the same change rule). Thus, the width-to-thickness ratio of the ductile casting should be between 7 and 10.

6. Conclusions

In this paper, an innovative energy dissipation brace was incorporated into the steel framed structures, namely, buckling-restrained braced steel frames with ductile castings. Two single-story single-span scaled specimens with two different axial force ratios were tested under cyclic loading. And the mechanical properties were examined, including the stress and failure modes, hysteretic behavior, energy dissipation capacity and skeleton curve. Moreover, a detailed FE analysis with different parameters was performed, and the corresponding design suggestions were given. The main conclusions are summarized as follows:

1. In the cyclic loading test, the ductile castings entered the plastic state before BRB, and BRB supplemented the energy dissipation. And most of the inelastic deformation was concentrated in the yielding segment of the ductile castings. The two scaled specimens developed the expected ductile failure of the ductile castings, while the beam and column were damage-free, showing excellent ductility and deformation abilities.
2. The variation trend of the stress distribution of the finite element analysis and the test results were similar to each other; thus, there was mutual verification. The hysteretic curve of the structure was full, and the energy dissipation coefficient of the test was close to 2.10. Therefore, the structure has stable energy dissipation performance and can dissipate a large amount of energy under an earthquake.
3. The axial force ratio and width-to-thickness ratio of the ductile casting have a great influence on the performance of the structure, as indicated by the finite element simulation. The effect of the outer restraint components reduced the influence of the yielding segment on the energy dissipation capacity of the structure. In addition, recommended value ranges of the design parameters were given.
4. The buckling-restrained brace with ductile castings was connected with frame by bolts can relieve the stress distribution in the beam–column region. And the bolt connection can effectively transmit force, the structure assembly and post-earthquake recoverability can be achieved as expected.

Acknowledgments

The financial supports from the National Natural Science Fund of China under grant No. 51968044 and No. 51568040, and the National Key Research and Development Program of China No. 2019YFD1101003 are gratefully acknowledged.

ORCID

Zhanzhong Yin https://orcid.org/0000-0003-3064-7158
Bo Yang https://orcid.org/0000-0001-9642-2088

References

Astaneh-Asl A, Goel SC, Hanson RD (1989) Cyclic behavior of double angle bracing members with end gusset plates. Research Report UMEE 8287, University of Michigan, Ann Arbor, MI, USA

Avci-Karatas C, Celik OC, Eruslu SO (2019) Modeling of buckling restrained braces (BRBs) using full-scale experimental data. *KSCE Journal of Civil Engineering* 23(10):4431-4444, DOI: 10.1007/s12205-019-2430-y

Avci-Karatas C, Celik OC, Yalcin C (2018) Experimental investigation of aluminum alloy and steel core buckling restrained braces (BRBs). *International Journal of Steel Structures-Springer* 18(2):650-673, DOI: 10.1007/s13296-018-0025-y

Balut N, Gioncu V (2003) Suggestion for an improved 'dog-bone' solution. Proceedings of the 4th international conference on behavior of steel structures in seismic areas, Naples, Italy

Barbagallo F, Bosco M, Marino EM, Rossi PP (2019) Achieving a more effective concentric braced frame by the double-stage yield BRB. *Engineering Structures* 186:484-497, DOI: 10.1016/j.engstruct.2019.02.028

Black RG, Wenger WAB, Popov EP (1980) Inelastic buckling of steel struts under cyclic load reversals. UCB/EERC-80/40, Earthquake Engineering Research Center, University of California, Berkeley, CA, USA

Chou CC, Liou GS, Yu JC (2012) Compressive behavior of dual-gusset-plate connections for buckling-restrained braced frames. *Journal of Constructional Steel Research* 76:54-67, DOI: 10.1016/j.jcsr.2012.03.003

Clark P, Kasai K (1999) Design procedures for buildings incorporating hysteretic damping devices. Proceedings 68th annual convention, October, Santa Barbara, CA, USA

El-Tayem AA, Goel SC (1985) Cyclic behavior of angle X - Bracing with welded connections. Research report UMCE 85-4, University of Michigan, Ann Arbor, MI, USA

Foutch DA, Goel SC, Roeder CW (1987) Seismic testing of a full scale

steel building. *Journal of Structural Engineering* 113(11):2111-2129, DOI: 10.1061/(ASCE)0733-9445(1987)113:11(2111)

Fujimoto M, Wada A, Saeki E, Watanabe A, Hitomi Y (1988) A study on the unboned brace encased in buckling-restraining concrete and steel tube. *Journal of Structural and Construction Engineering* 34B:249-258

GB 50011-2010 (2016) Code for seismic design of buildings. GB 50011-2010, China Ministry of Construction, Beijing, China (in Chinese)

GB 50017-2017 (2017) Standard for design of steel structures. GB 50017-2017, China Ministry of Construction, Beijing, China (in Chinese)

Gray MG, Christopoulos C, Packer JA (2010) Cast steel yielding fuse for concentrically braced frames. Proceeding of the 9th US National and 10th Canadian conference on earthquake engineering, July 25-29, Ottawa, ON, Canada

Gray MG, Christopoulos C, Packer JA (2014) Cast steel yielding brace system for concentrically braced frames: Concept development and experimental validations. *Journal of Structural Engineering* 140(4):1-11, DOI: 10.1061/(ASCE)ST.1943-541X.0000910

Guo YL, Wang XA, Jiang LX (2010) Design theory of assembled buckling-restrained braces and buckling-restrained braced frames. *Structural Engineers* 26(6):164-176, DOI: 10.15935/j.cnki.jggcs.2010.06.026 (in Chinese)

Hoveidae N, Rafezy B (2012) Overall buckling behavior of all-steel buckling restrained braces. *Journal of Constructional Steel Research* 79:151-158, DOI: 10.1016/j.jcsr.2012.07.022

Hsiao PC (2012) Seismic performance evaluation of concentrically braced frames. PhD Thesis, University of Washington, Seattle, WA, USA

Jia MM, Zhang SM, Lu DG, Jiang SL (2009) Influence of layout principle of buckling-restrained braces on aseismic performance of steel frame. *Engineering Mechanics* 26(7):140-146 (in Chinese)

JGJ/T 101-2015 (2015) Specification for seismic test of buildings. JGJ/T 101-2015, China Ministry of Construction, Beijing, China (in Chinese)

Lehman D, Roeder C (2008) Improved seismic design of concentrically braced frames and gusset plate connections. Structures congress 2008, April 24-26, Vancouver, BC, Canada, DOI: 10.1061/41016(314)258

Li JM (2019) Experimental study on buckling restrained brace with ductile connectors. MSc Thesis, Lanzhou University of Technology, Lanzhou, China (in Chinese)

Piedrafita D, Cahis X, Simon E, Comas J (2015) A new perforated core buckling restrained brace. *Engineering Structural* 85:118-126, DOI: 10.1016/j.engstruct.2014.12.020

Popov EP, Takanashi K, Roeder CW (1976) Structural steel bracing systems: Behavior under cyclic loading. EERC Report 76-17, University of California, Berkeley, CA, USA

Powell JA (2009) Evaluation of special concentrically braced frames for improved seismic performance and constructability. MSc Thesis, University of Washington, Seattle, WA, USA

Roeder CW, Lehman DE, Clark K, Powell J, Yoo JH, Tsai KC, Lin CH, Wei CY (2011a) Influence of gusset plate connection and braces on the seismic performance of X-braced frames. *Earthquake Engineering and Structural Dynamics* 40(4):355-374, DOI: 10.1002/eqe.1024

Roeder CW, Lumpkin EJ, Lehman DE (2011b) A balanced design procedure for special concentrically braced frame connections. *Journal of Constructional Steel Research* 67(11):1760-1772, DOI: 10.1016/j.jcsr.2011.04.016

Stevens D, Wiebe L (2019) Experimental testing of a replaceable brace module for seismically designed concentrically braced steel frames. *Journal of Structural Engineering* 145(4):1-11, DOI: 10.1061/(ASCE)ST.1943-541X.0002283

Tremblay R, Filiatrault A, Timler P (1995) Performance of steel structures during the 1994 northridge earthquake. *Canadian Journal of Civil Engineering* 22(2):338-360, DOI: 10.1016/0148-9062(96)87657-1

Tsai KC, Lai JW, Hwang YC, Lin SL (2004) Research and application of double-core buckling restrained braces in Taiwan. 13th world conference on earthquake engineering, August 1-6, Vancouver, BC, Canada

Uriz P (2005) Toward earthquake-resistant design of concentrically braced steel frame structures. PhD Thesis, University of California, Berkeley, CA, USA

Uriz P, Mahin S (2004) Seismic performance assessment of concentrically braced steel frames. Proceedings of the 13th world conference on earthquake engineering, August 1-6, Vancouver, BC, Canada

Wakabayashi M (1972) Experiments on the elastic-plastic behavior of bars subjected to cyclic axial loads. Proceedings of annual meeting, October, Japan

Ward KM, Fleischman RB, Federico GA (2012) A cast modular bracing system for steel special concentrically braced frames. *Engineering Structural* 45:104-116, DOI: 10.1016/j.engstruct.2012.05.025

Xu PX (1990) Behavior of double channel bracing members under large cyclic deformations. PhD Thesis, University of Michigan, Ann Arbor, MI, USA

Yin ZZ, Pan CC (2018) Parameter analysis of buckling restrained brace with steel casting under unidirectional loading. *Steel Construction* 33(07):9-15, DOI: 10.13206/j.gjg201807002 (in Chinese)

Yin ZZ, Xu DY, Yang B (2020) Experimental study of prefabricated buckling-restrained braces with ductile casting connectors. *Journal of Building Structures*, DOI: 10.14006/j.jzjgxb.2020.0261 (in Chinese)

Zhao Y, Guo YL (2010) Research on design method of buckling restrained braced frames. *Building Structure* 40(01):38-43+85, DOI: 10.19701/j.jzjg.2010.01.009 (in Chinese)